Characterization of Carrier Transport Using a Bifacial Structure for Rational Design of p-n Junction PbS Solar Cells

Matthew Duff, Sumin Bae, and Jung-Kun Lee

Department of Mechanical Engineering & Material Science, University of Pittsburgh, Pittsburgh, PA 15261, USA

Abstract

In this study, a difference in the mobility of holes and electrons as a minority carrier has been systematically characterized in PbS quantum dot (QD) solar cells. While the mobility of electrons and holes is important in designing the p-n junction solar cells, it is still challenging to measure them during the normal operation of QD solar cells. We fabricated the bifacial solar cells and characterized the carrier transport by measuring the decay of photocurrent under pulsed illumination. The electron and hole mobility of p-type, n-type, and p-n junction type PbS QD film was examined and its connection to the performance of the solar cells was studied. In n-type PbS layer, the diffusion length of both electron and hole is ~300 nm. In contrast, the diffusion length of hole and electron of p-type PbS layer is 250 nm and 175 nm. The asymmetric charge kinetics between holes and electrons in p-type PbS has been further elucidated when the active layer thickness of the solar cells is altered. This result offers a rationale design rule of p-n junction type QD solar cells.

keyword: PbS quantum dot, solar cells, carrier mobility, bifacial structure, transparent conducting film

1. Introduction:

Quantum dot (QD) films have been extensively studied for their unique physical properties and applications to energy harvesting and display devices. A change in the particle size modifies the electronic band structure and increases a light absorption coefficient. Combined with multiple exciton generation and inexpensive solution processing, QD films can lead to affordable solar cells which have a potential to break the Shockley - Queisser limit. [1] The efficiency of PbS QD devices has increased to 13.3 % (16.6 % for ammonium lead triiodide QD devices) which is still lower than the theoretical efficiency ~ 30%.[2-4] This gap is partially due to a tradeoff between light absorption and charge transport. While all solar cells have such a problem, the unique carrier hopping in QD films limits the charge transport and makes this tradeoff more pronounced. To increase the carrier mobility and decrease the recombination rate, the surface passivation, impurity content, and crystallinity of QDs have been carefully controlled. [5-10]

One more important issue which has not been systematically studied yet in QD solar cells is a difference in the mobility of holes and electrons as a minority carrier. [10-13] A design of p-n junction solar cells can be optimized by taking into account the difference in the minority carrier mobility. For example, if the hole mobility is smaller than the electron mobility, the n-type layer needs to be thinner than the p-type layer to minimize the recombination of photogenerated carriers. [10, 14-17] Therefore, for semiconductors with asymmetric hole and electron transport behavior, revising device architecture becomes an avenue of improving charge transport and suppressing carrier recombination. [5, 18] However, it is still challenging to measure the mobility of electrons and holes during the normal operation of QD solar cells. Traditionally, the carrier mobility is measured by using Hall effect measurement technique or fabricating a field-effect transistor. [19-28] However, the Hall effect measurement provides only the majority carrier mobility. In addition, the minority carrier mobility in the field-effect-transistor is always larger than the minority carrier mobility in the solar cells, since the minority carrier travels in a channel where the majority carriers are depleted. [21, 31] Another way to characterize the carrier transport in the solar cells is to measure the decay of photocurrent under pulsed illumination. [32-34] Since the decay measurement is

performed in an operating condition of the solar cells, the measured data are more realistic and beneficial to the design of the solar cells. However, it is difficult to quantitatively separate the mobility of electrons and holes in the decay measurement using traditional solar cells where both effects are intermixed.

The unique approach in the study is the design and fabrication of a bifacial architecture of the QD solar cells, which allows for illumination through both the front and back sides of the solar cells. By varying the illumination direction, either hole or electron diffuses a much longer distance to reach the respective collecting electrode. This controls the overall current decay behavior. In other words, by changing illumination direction, the carrier transport in the solar cell shifts between either a hole or electron diffusion-limited mode. This is schematically explained in Figure 1. The new bifacial architecture enables us to quantitatively characterize the transport of both majority and minority carriers in the same QD film during the normal solar cell operation. In this study, we measured electron and hole mobility in p-type, n-type, or p-n junction type PbS QD film and found a correlation between the performance and device structure of p-n junction PbS QD solar cells. In p-type PbS QD film capped with thiol ligands, holes travel longer than electrons. In n-type PbS QD film capped with iodine ligands, the electron mobility is similar to hole mobility and the diffusion length of both carriers is ~300 nm. The diffusion length of holes and electrons turns out 250 nm and 175 nm, respectively. The asymmetric charge kinetics between holes and electrons in p-type PbS has been further elucidated by altering the active layer thickness of the solar cells, which offers a rationale design rule of p-n junction type QD solar cells.

2. Experimental Procedures:

2-1. PbS quantum dot fabrication

High purity octadecene (ODE), PbO, oleic acid (OA), bis(trimethylsilyl) sulfide (TMS) were purchased through Fisher Scientific. Prior to synthesis ODE was degassed in a vacuum at 85 ºC for 12 hours. PbS QDs with an absorption peak of λ = 900 nm were fabricated by adjusting a synthesis technique pioneered by Hines and Scholes. [35] 450 mg of PbO, 18 ml of ODE, and 1.5 ml of OA were mixed in a three neck

flask in a vacuum at 70 ºC for 3 hours. Then, the air in the flask and Schlenk line was switched to nitrogen, and the solution was heated at 95 ºC for 1 hour until the mixture became clear. The Pb precursor solution was further reacted at 115 ºC in an oil bath. The flask was removed from the bath while the temperature of the inside solution was monitored with an embedded thermal couple. To initiate the nucleation of PbS QDs, 10 ml of ODE and 207 uL of TMS were swiftly injected into the PbO-oleate mixture inside the flask using a syringe. This decreased the temperature quickly and black PbS QDs appeared. The solution cooled naturally to room temperature in a nitrogen atmosphere. After acetone was added to the solution, QDs were separated by centrifuging and redispersed in hexane. The UV/Vis absorption spectra of PbS QDs were measured and the band gap and size of PbS QD were estimated from the UV/Vis absorption spectra. The bandgap of PbS QDs is1.37 eV which corresponds to 3.15 nm. Prior to PbS film deposition, PbS QDs were further washed and centrifuged using a mixture of acetone and methanol. This washing process was repeated three times. The PbS QDs were redispersed in hexane at a concentration of 25mg/ml and stored in a low humidity desiccator.

2-2. Fabrication of PbS solar cells

Fluorine doped tin oxide (FTO) film on the glass was used as a transparent and conductive bottom contact for solar cells. The FTO substrate was patterned by wet etching in a mixture of zinc powder and HCl (18% in water) for 30 seconds. Patterned FTO substrates were cleaned through sequential sonication in acetone, DI water, and ethanol for 20 minutes each. Cleaned substrates were dried and treated in a deep UV/ozone chamber for 20 minutes. A 20 nm TiO_2 layer (an electron transport layer) was then deposited on the patterned FTO substrates using ozone assisted atomic layer deposition (ALD) at 250 ºC. Tetrakis(dimethylamido)titanium (TDMA-Ti) and O_3 were used as precursors. To form p-type PbS QD layer, PbS QDs were spin-coated on patterned FTO substrate in low humidity, nitrogen filled glove box. The substrates were spin-coated with 40 μl of PbS solution (25 mg PbS in 1 ml hexane) at 2500 rpm. For p-type PbS film, 80 μl of 2 V/V% of 1,2- ethanedithiol (EDT) in acetonitrile was cast onto PbS QD layer to exchange the native oleates with short thiols and 80 μl of acetonitrile was cast on the spinning substrate

to remove residual ligands and clean the film. For n-type PbS QD film, 80 μl of 10mg/ml of tetra-n-butylammonium iodide (TBAI) in methanol was used to exchange the native oleate ligands with iodine ions. After a cycle of the coating process, 20 nm thick PbS QD film was obtained. The coating was repeated to reach a target thickness (200 nm). The top transparent electrode has a sandwich structure of semiconductor-metal-semiconductor. 10 nm thick MoO_3, 10 nm thick Au, and 10 nm thick MoO_3 were deposited sequentially to form a conductive transparent multilayer contact for hole transfer, which is called MAM hereafter. [36-38] The active area of the solar cell was 0.0375 cm^2 (1.5 × 2.5 mm) which was controlled by the overlap of electrodes on the top and bottom of PbS QD layer.

2-3. Characterization of PbS solar cells

To examine the transport behavior of holes and electrons, a dual illumination technique was employed. The measurement configuration is schematically shown in Figure S1. The solar cells were illuminated through the top or bottom transparent electrode. To keep the incident light spectra constant between illumination directions, different light filters were used. If the light intensity is not the same, it is difficult to form a quantitative comparison as different amounts of photogenerated carriers affect the carrier transport. The measurement configuration where the light goes through the top transparent electrode first before reaching PbS, is called top illumination. If the light goes through the FTO electrode first before reaching PbS, the measurement configuration is called bottom illumination. Figure S2 shows the absorbance of light by the solar cell for both illumination directions. UV/Vis absorption spectra are similar and a different in the light intensity is less than 3%, which indicates that the illumination direction does not change the amount of solar energy absorbed by PbS film. At both top and bottom illumination configurations, voltage and current decay measurements were done using the stepped light-induced transient measurements of photocurrent and photovoltage (SLIM-PCV) method. [39-41] A monochromatic of a laser diode (λ=445 nm) was controlled by a function generator (Agilent 33220A). Voltage decay of the PbS solar cell was monitored by a digital storage oscilloscope (Tektronix, TDS2024B) that was synchronized with a function generator. A current amplifier connecting the sample and the oscilloscope was set up for current decay measurements. The

average charge carrier lifetime was extracted from the decay constant of the voltage decay curve. A diffusion coefficient was calculated from the current decay measurements using an equation (1):

$$D = \frac{l^2}{2.37\tau} \qquad (1)$$

where l is the thickness of the PbS film and τ is the current decay constant. Mobility can then be calculated using the Einstein kinetics relation in an equation (2):

$$D = \frac{\mu_q k_b T}{q} \qquad (2)$$

3. Results and Discussion:

3-1. Transport kinetics of holes and electrons in n-type and p-type PbS films

A difference in the surface passivation by ligands greatly changes the electrical properties of PbS QD films. EDT and TBAI ligands leave sulfur and iodine ions onto the surface of PbS QDs. The addition of the iodine impurity onto the PbS surface generates free electrons and impart n-type conductivity. The sulfur impurity on the PbS surface generates a hole and results in p-type PbS. Figure 2 shows J-V curves of only p-type or only n-type PbS QD solar cells under the top or bottom illumination. Performance parameters of solar cells are summarized in Table 1. J_{SC} of n-type PbS solar cells (21.1 mA/cm^2 for the bottom illumination) is larger than that of p-type PbS solar cells (16.7 mA/cm^2). The effect of the illumination direction on J_{SC} is more significant in p-type PbS (16.7 vs 12.1 mA/cm^2) than marginal in n-type PbS solar cells (21.1 vs 19.1 mA/cm^2). Since the light absorbance of PbS film is almost the same for all cases, changes in the photocurrent indicate that the type of PbS QDs and the illumination direction have an impact on the transport and recombination of photogenerated carriers. V_{OC} does not depend on the illumination direction but is mainly determined by the major carrier type of PbS. V_{OC} of n-type PbS solar cells is 0.43 - 0.44V which is smaller than that of p-type PbS solar cells (0.61 – 0.63 V). This is due to the Fermi energy difference between p-type PbS and n-type PbS. In p-type PbS solar cells, the maximum V_{OC} is same as a

difference in Fermi energy levels between n-type TiO_2 and p-type PbS. In n-type PbS solar cells, the maximum V_{OC} is determined by a difference in Fermi energy levels between n-type TiO_2 and p-type MoO_3, which is 0.48 V. This is close to the measurement result (0.43 - 0.44V) of n-type PbS solar cells. [42-44]

Figure 3 shows the transient current decay results of the SLIM-PCV measurements of p-type and n-type type devices under chopped illumination from the FTO or MAM side. The transient decay times of the FTO and MAM illuminations are nearly identical (~2.3 μsec) in the n-type PbS solar cell. In contrast, the p-type PbS solar cell shows a clear dependence on the illumination direction. The MAM side illumination takes a much longer time (~7.0 μsec) to reach zero current than the FTO side illumination (~3.6 μsec). As shown in Figure 1, a major difference between FTO and MAM illumination is how far electrons and holes travel to reach conductive electrodes (FTO or MAM). In the case of FTO illumination, the majority of excess carriers are generated near the TiO_2 - PbS interface, and photogenerated holes can travel a longer distance than photogenerated electrons to reach the electrode. This suggests that hole transport kinetics limits the carrier transport for the FTO illumination. When light is illuminated from the MAM side, the exact opposite occurs; electrons travel farther than holes, and electron transport limits the transport of photogenerated carriers. Diffusion coefficient and carrier mobility are shown in table 3. Diffusion coefficient are calculated from Figure 3 and mobility are obtained using Einstein relation. [29,30] Table 3 indicates that 1) photogenerated carriers move faster in n-type PbS film than p-type solar cells, 2) holes and electrons move at a similar velocity in n-type PbS film, and 3) holes moves faster than electrons in p-type PbS film.

A change in the carrier transport velocity affects the carrier collection efficiency since a decrease in the transport velocity increases the recombination probability of photogenerated carriers. Figure 4 shows IPCE spectra of PbS solar cells illuminated from two different directions. In p-type PbS QD solar cell exhibiting very different electrons and hole transport kinetics, the quantum efficiency of the FTO illumination is distinguished from that of MAM illumination. In addition, there is a noticeable effect of the light wavelength on the IPCE. At λ = 400 nm where the light is absorbed near the incident surface of the

solar cells, the quantum efficiency of p-type solar cell is 75% for FTO illumination and 25% for MAM illumination. This verifies the slow electron transport in p-type PbS. However, two IPCE curves of the n-type PbS solar cell in Fig. 4(b) have a similar shape. This is consistent with Figure 3 showing that electrons and holes have a similar velocity in n-type PbS film.

3-2. Carrier transport kinetics in p-n junction type PbS QD solar cells

A very important mechanism enhancing the carrier transport of PbS QD solar cells is to use the drift of carriers at the junction between p-type and n-type layers where majority carriers are depleted. In this study, we also examined how the addition of the p-n junction affects the carrier transport behavior in PbS films. Figure 5 shows J-V curves of p-n junction PbS solar cells with different junction locations. A cross section of PbS QD solar cells is schematically shown in Figure 5(a). Performance parameters of solar cells are summarized in Table 2. Compared with n-type PbS, 80-20 n/p PbS exhibits increase in J_{sc} (from 21.10 mA/cm^2 to 22.27 mA/cm^2 at the FTO illumination condition) and V_{oc} (from 0.44 V to 0.55 V) by 5 % and 25 %, respectively. In 20-80 n/p PbS, the addition of a thin n-type layer increases J_{sc} (from 16.68 mA/cm^2 to 19.10 mA/cm^2) by 14 % and decreases V_{oc} (from 0.61 V to 0.57 V) by 7 %. The addition of p-n junction suppresses the carrier recombination and its effect is more pronounced in p-type PbS which suffers from the slow transport of electrons. Less misalignment of E_C and E_V of 20-80 n/p PbS, FTO and MAM mitigates the potential loss of carriers at the PbS-electrode interfaces. It is noted that an increase in the thickness ratio of n-type PbS decreases a difference in J_{SC} between MAM and FTO illumination. The ratio of J_{SC} from FTO illumination over J_{SC} from MAM illumination is 68% for 20-80 n/p PbS and 89% for 80-20 n/p PbS, which is attributed to the similar transport velocity of electrons and holes of n-type PbS film.

To quantitatively examine the kinetics of hole and electron transport in p-n junction devices, the transient current decay measurements were also performed using the dual light illumination technique. Figure 6 shows the current decay curves of PbS films with different thickness ratios of n- and p-type PbS layers. As the thickness ratio of n-type PbS increases, the decay constant decreases and the effect of the illumination direction is reduced. The addition of n-layer enhances the transport of both electrons and holes

in the p-n junction devices. The potential barrier at the interface between the n-type and p-type layers also facilitates the carrier transport through the drift mechanism. In addition, a change in the decay time in Figure 6 is inversely proportional to J_{sc} of the solar cells in Figure 5, since a fast transport of carriers improves the carrier collection efficiency. This clearly indicates the usefulness of the transient decay measurement in analyzing the performance of thin film solar cells. IPCE spectra shown in Figure S3 confirm the importance of the carrier transport in the photon-electron conversion process and attests to the difference between hole and electron transport kinetics. The thicker the p-type layer, the more notable effect of the illumination direction is observed in the wavelength range of 400 - 500 nm. This is due to the imbalanced transport of electrons and holes. Since the electron transport is much slower than the hole transport in the p-type layer, the illumination direction into 20-80 n/p PbS has a large impact on the photons of the short wavelength, which are mostly absorbed near the entering surface of p-type PbS film. In contrast, both electrons and holes move fast in 80-20 n/p PbS and IPCE spectra of FTO and MAM illuminations are similar. In the long wavelength range, photons go to the deeper part of PbS film and a difference in the transport length of electrons and holes is decreased, leading to the marginal effect of the illumination direction on IPCE.

4. Conclusion:

The difference in hole and electron transport in PbS solar cells was measured using the unique dual illumination technique. This structure enables the independent measurement of the mobility of electrons and holes during the normal operation of solar cell devices. A change in the illumination direction of the bifacial cells switches the carrier transport to either a hole or electron diffusion-limited mode. While holes travel faster than electrons in only p-type PbS solar cells, the difference between electron and hole mobility is small in only n-type PbS solar cells. The asymmetric charge kinetics between holes and electrons in p-type PbS has been further elucidated by altering the active layer thickness of the solar cells. This study

provide a guideline to measure the electron and hole mobility in operating solar cells and design the p-n junction type QD solar cells of a high solar energy conversion efficiency.

Acknowledgement

This work was supported by National Science Foundation, USA (NSF 1709307), Korea Institute of Energy Technology Evaluation and Planning (KETEP) grant funded by the Korea government (MOTIE) (20193091010460).

Table 1. Performance of solar cells of only p-type PbS or only n-type PbS under top illumination or bottom illumination (a relative thickness ratio of n- and p-type PbS layer is 10:0 for 100-0 n/p and 0:10 for 0-100 n/p solar cell).

PbS Solar Cells	**J_{sc} (mA/cm^2)**	**V_{oc} (V)**	**η (%)**	**FF**
100-0 n/p: bottom illumination	21.10	0.44	3.47	0.37
100-0 n/p: top illumination	19.12	0.43	3.10	0.37
0-100 n/p: bottom illumination	16.68	0.61	4.35	0.43
0-100 n/p: top illumination	12.12	0.63	3.28	0.43

Table 2. Performance of p-n junction type PbS under top illumination or bottom illumination (a relative thickness ratio of n- and p-type PbS layer is 2:8 for 20-80 n/p solar cell, 5:5 for 50-50 n/p solar cell, and 8:2 for 80-20 n/p solar cell).

PbS Cell	J_{sc} (mA/cm^2)	V_{oc} (V)	η (%)	FF
80-20 n/p-FTO illumination	22.27	0.55	5.37	0.43
80-20 n/p-MAM illumination	19.82	0.56	4.88	0.44
50-50 n/p-FTO illumination	21.03	0.56	5.18	0.45
50-50 n/p-MAM illumination	18.33	0.57	4.53	0.44
20-80 n/p-FTO illumination	19.10	0.57	4.82	0.45
20-80 n/p-MAM illumination	15.06	0.58	3.33	0.43

Table 3. Diffusion coefficient and converted mobility of p-type PbS and n-type PbS films.

PbS Type	Diffusion Coefficient (cm^2/s)		Mobility (cm^2/Vs)		Diffusion Length (nm)	
	Electron	**Hole**	**Electron**	**Hole**	**Electron**	**Hole**
p-type	1.48E-05	3.00E-05	5.77E-04	1.17E-03	175	250
n-type	4.75E-05	4.50E-05	1.85E-03	1.75E-03	310	300

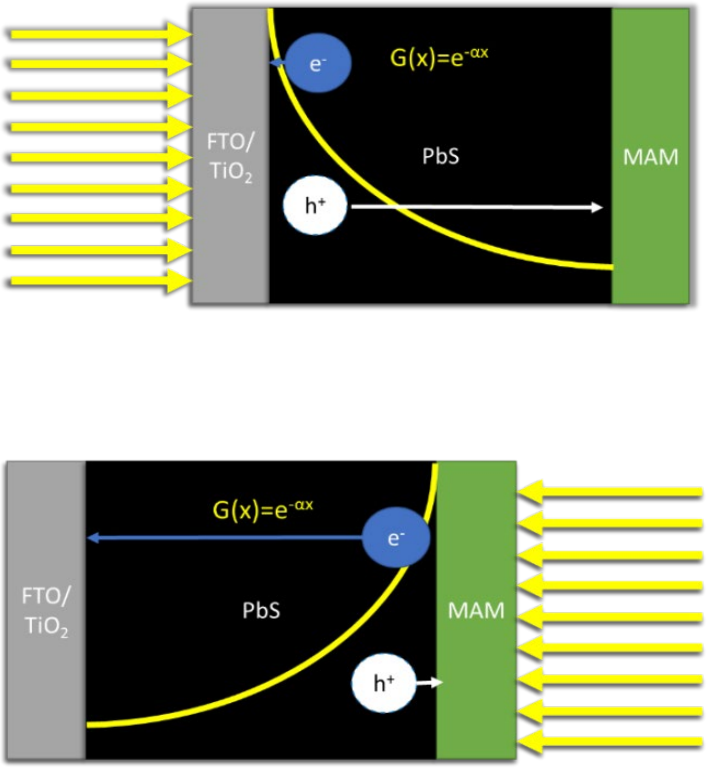

Figure 1. Schematic explanation of the dual illumination test showing the charge generation and subsequent transport of electrons and holes (G(x): a carrier generation rate as a function of a distance (x) from the light entrance interface of PbS film); (top) when light is illuminated through the fluorine doped tin oxide (FTO)/TiO_2 side, holes need to travel longer distance to be converted to electricity and hole diffusion controls the overall transport of photogenerated carriers, (bottom) when light is illuminated through the MoO_3/Au/MoO_3 (MAM) side, electron diffusion is important in the overall transport of photogenerated carriers.

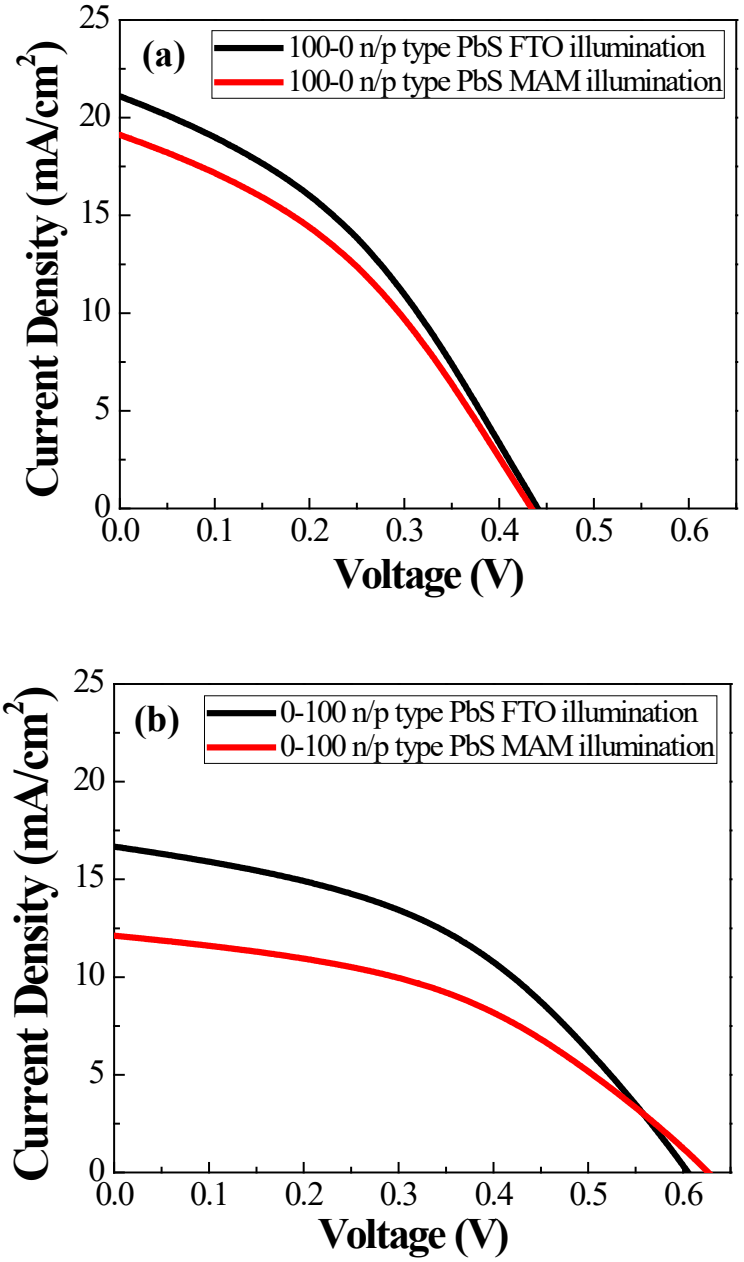

Figure 2. J - V curves of 200 nm thick PbS QD solar cells under continuous illumination from FTO or MAM side; a) only p-type PbS QD solar cells (100-0 n/p type), b) only n-type PbS QD solar cells (0-100 n/p type).

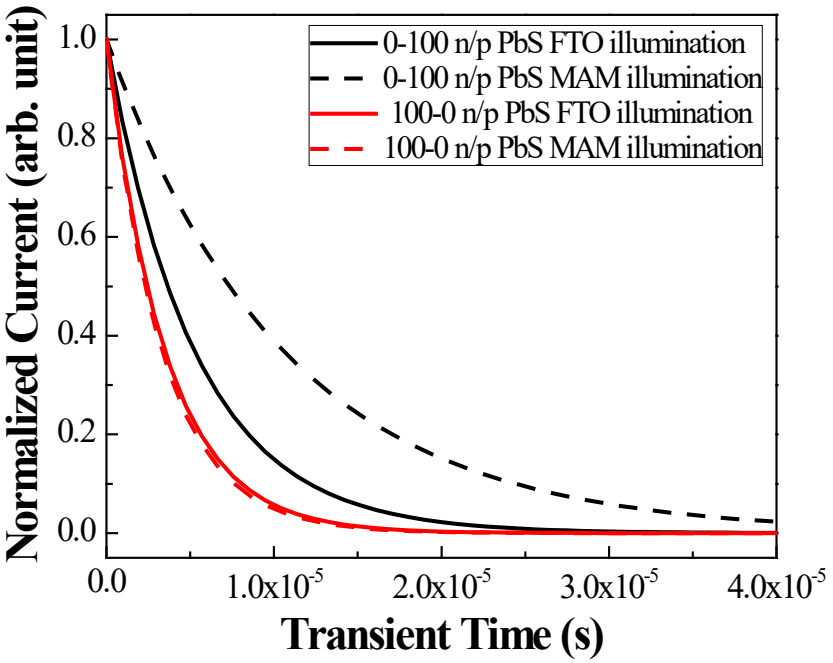

Figure 3. Transient current curves of only p-type (0-100 n/p) or only n-type (100-0 n/p) PbS QD solar cells under pulsed illumination from FTO or MAM side.

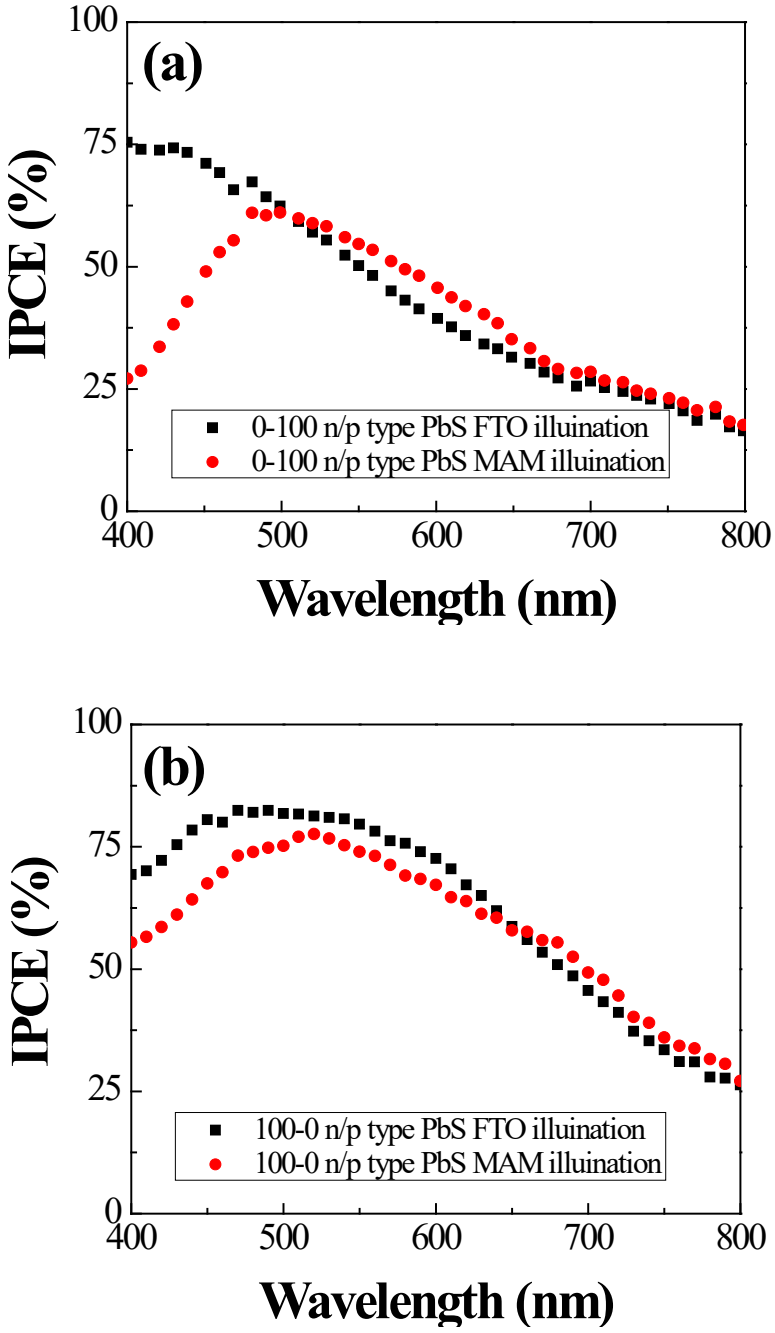

Figure 4. IPCE spectra under continuous illumination from FTO or MAM side; (a) only p-type QD solar cells, (b) n-type PbS QD solar cells.

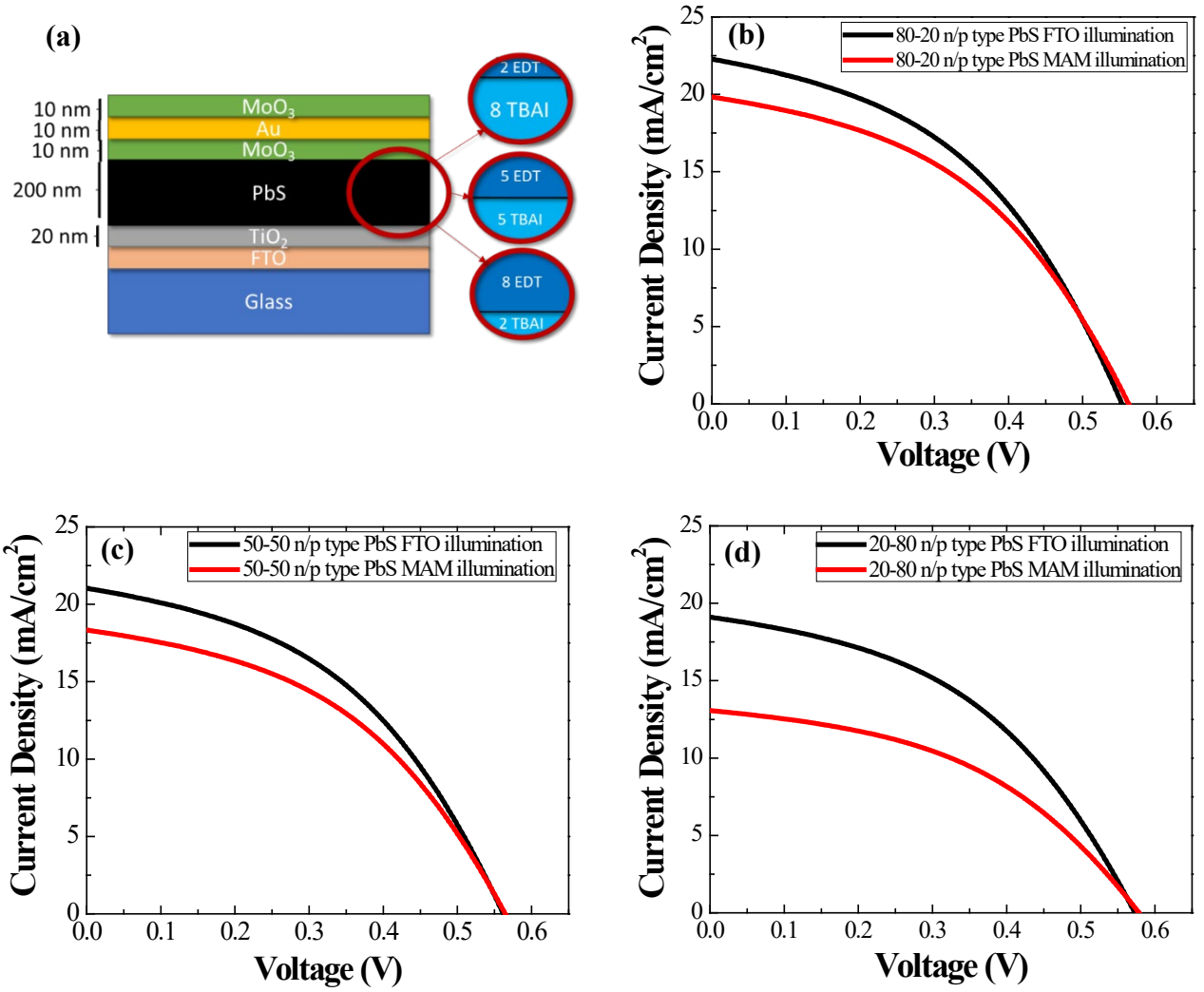

Figure 5. J-V curves of fabricated PbS solar cells containing p-n junction under the top and bottom illuminations. The 200 nm thick PbS active layer consists of p- and n-type PbS layers of different thickness ratios. A relative thickness ratio of n- and p-type PbS layer is 8:2 for 80-20 n/p solar cell (160 nm thick n-layer/40 nm thick p-layer), 5:5 for 50-50 n/p solar cell (100 nm thick n-layer/100 nm thick p-layer), and 2:8 for 20-80 n/p solar cell (40 nm thick n-layer/160 nm thick p-layer).

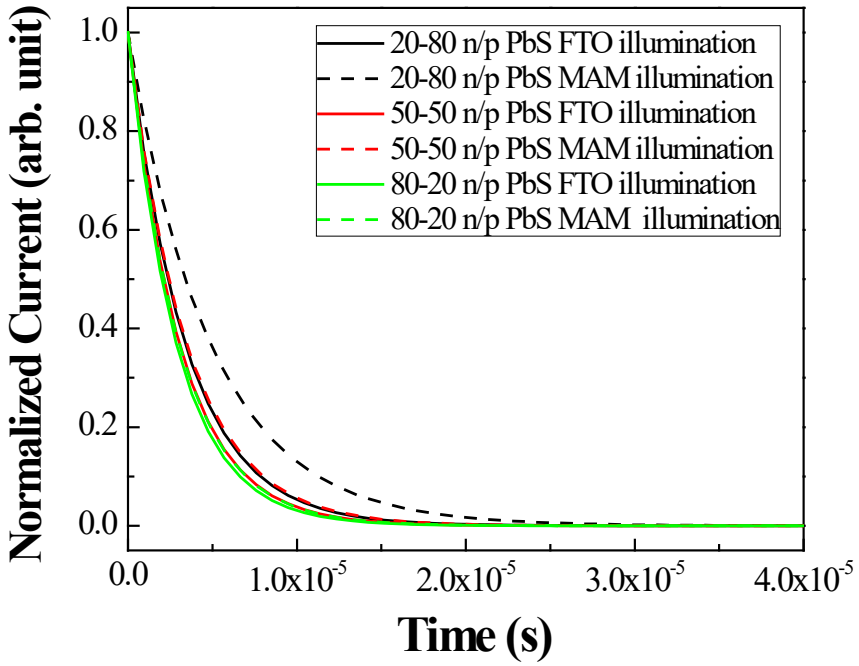

Figure 6. Transient current curves of p-n junction type PbS solar cells. The 200 nm thick PbS active layer consists of p- and n-type PbS layers of different thickness ratios. A relative thickness ratio of n- and p-type PbS layer is 8:2 for 80-20 n/p solar cell (160 nm thick n-layer/40 nm thick p-layer), 5:5 for 50-50 n/p solar cell (100 nm thick n-layer/100 nm thick p-layer), and 2:8 for 20-80 n/p solar cell (40 nm thick n-layer/160 nm thick p-layer).

References:

[1] R.J. Ellingson, M.C. Beard, J.C. Johnson, P. Yu, O.I. Micic, A.J. Nozik, A. Shabaev, A.L. Efros, Highly Efficient Multiple Exciton Generation in Colloidal PbSe and PbS Quantum Dots, Nano Letters 5(5) (2005) 865-871.

[2] J. Xu, O. Voznyy, M. Liu, A.R. Kirmani, G. Walters, R. Munir, M. Abdelsamie, A.H. Proppe, A. Sarkar, F.P. García de Arquer, M. Wei, B. Sun, M. Liu, O. Ouellette, R. Quintero-Bermudez, J. Li, J. Fan, L. Quan, P. Todorovic, H. Tan, S. Hoogland, S.O. Kelley, M. Stefik, A. Amassian, E.H. Sargent, 2D matrix engineering for homogeneous quantum dot coupling in photovoltaic solids, Nature Nanotechnology 13(6) (2018) 456-462.

[3] M.J. Choi, F.P.G. de Arquer, A.H. Proppe, A. Seifitokaldani, J. Choi, J. Kim, S.W. Baek, M.X. Liu, B. Sun, M. Biondi, B. Scheffel, G. Walters, D.H. Nam, J.W. Jo, O. Ouellette, O. Voznyy, S. Hoogland, S.O. Kelley, Y.S. Jung, E.H. Sargent, Cascade surface modification of colloidal quantum dot inks enables efficient bulk homojunction photovoltaics, Nat Commun 11(1) (2020).

[4] M.M. Hao, Y. Bai, S. Zeiske, L. Ren, J.X. Liu, Y.B. Yuan, N. Zarrabi, N.Y. Cheng, M. Ghasemi, P. Chen, M.Q. Lyu, D.X. He, J.H. Yun, Y. Du, Y. Wang, S.S. Ding, A. Armin, P. Meredith, G. Liu, H.M. Cheng, L.Z. Wang, Ligand-assisted cation-exchange engineering for high-efficiency colloidal Cs(1-x)FA(x)PbI(3) quantum dot solar cells with reduced phase segregation, Nat Energy 5(1) (2020) 79-88.

[5] S.-H. Turren-Cruz, M. Saliba, M.T. Mayer, H. Juárez-Santiesteban, X. Mathew, L. Nienhaus, W. Tress, M.P. Erodici, M.-J. Sher, M.G. Bawendi, M. Grätzel, A. Abate, A. Hagfeldt, J.-P. Correa-Baena, Enhanced charge carrier mobility and lifetime suppress hysteresis and improve efficiency in planar perovskite solar cells, Energy & Environmental Science 11(1) (2018) 78-86.

[6] M.L.A. Aguilera, C.H. Vasquez, M.A.G. Trujillo, J.M.F. Marquez, S.G. Hernandez, G.S.C. Puente, Blue CdTe surface obtained by CdCl2 thermal treatment and their performance on CdTe solar cell, 2018 IEEE 7th World Conference on Photovoltaic Energy Conversion (WCPEC) (A Joint Conference of 45th IEEE PVSC, 28th PVSEC & 34th EU PVSEC), 2018, pp. 0812-0817.

[7] I.A. Sahito, F. Ahmed, Z. Khatri, K.C. Sun, S.H. Jeong, Enhanced ionic mobility and increased efficiency of dye-sensitized solar cell by adding lithium chloride in poly(vinylidene

fluoride) nanofiber as electrolyte medium, Journal of Materials Science 52(24) (2017) 13920-13929.

[8] E.M. Sanehira, A.R. Marshall, J.A. Christians, S.P. Harvey, P.N. Ciesielski, L.M. Wheeler, P. Schulz, L.Y. Lin, M.C. Beard, J.M. Luther, Enhanced mobility CsPbI₃ quantum dot arrays for record-efficiency, high-voltage photovoltaic cells, Science Advances 3(10) (2017) eaao4204.

[9] Y. Ding, M. Sugaya, Q. Liu, S. Zhou, T. Nozaki, Oxygen passivation of silicon nanocrystals: Influences on trap states, electron mobility, and hybrid solar cell performance, Nano Energy 10 (2014) 322-328.

[10] E.J.W. Crossland, N. Noel, V. Sivaram, T. Leijtens, J.A. Alexander-Webber, H.J. Snaith, Mesoporous TiO2 single crystals delivering enhanced mobility and optoelectronic device performance, Nature 495(7440) (2013) 215-219.

[11] L. Hu, A. Mandelis, X. Lan, A. Melnikov, S. Hoogland, E.H. Sargent, Imbalanced charge carrier mobility and Schottky junction induced anomalous current-voltage characteristics of excitonic PbS colloidal quantum dot solar cells, Solar Energy Materials and Solar Cells 155 (2016) 155-165.

[12] G. Hodes, P.V. Kamat, Understanding the Implication of Carrier Diffusion Length in Photovoltaic Cells, J Phys Chem Lett 6(20) (2015) 4090-2.

[13] P. Heremans, D. Cheyns, B.P. Rand, Strategies for Increasing the Efficiency of Heterojunction Organic Solar Cells: Material Selection and Device Architecture, Accounts of Chemical Research 42(11) (2009) 1740-1747.

[14] T. Salim, S. Sun, Y. Abe, A. Krishna, A.C. Grimsdale, Y.M. Lam, Perovskite-based solar cells: impact of morphology and device architecture on device performance, Journal of Materials Chemistry A 3(17) (2015) 8943-8969.

[15] F. Zhao, L. Deng, K. Wang, C. Han, Z. Liu, H. Yu, J. Li, B. Hu, Surface Modification of SnO2 via MAPbI3 Nanowires for a Highly Efficient Non-Fullerene Acceptor-Based Organic Solar Cell, ACS Applied Materials & Interfaces 12(4) (2020) 5120-5127.

[16] G. Liu, H. Wang, M. Wang, W. Liu, R.E. Anugrah Ardhi, D. Zou, J.K. Lee, Study on a stretchable, fiber-shaped, and TiO2 nanowire array-based dye-sensitized solar cell with electrochemical impedance spectroscopy method, Electrochimica Acta 267 (2018) 34-40.

[17] H. Cai, J. Li, X. Xu, H. Tang, J. Luo, K. Binnemans, J. Fransaer, D.E. De Vos, Nanostructured composites of one-dimensional TiO2 and reduced graphene oxide for efficient dye-sensitized solar cells, Journal of Alloys and Compounds 697 (2017) 132-137.

[18] W. Qarony, M.I. Hossain, A. Tamang, V. Jovanov, A. Salleo, D. Knipp, Y.H. Tsang, Enhancing the energy conversion efficiency of low mobility solar cells by a 3D device architecture, Journal of Materials Chemistry C 7(33) (2019) 10289-10296.

[19] K.S. Jeong, J. Tang, H. Liu, J. Kim, A.W. Schaefer, K. Kemp, L. Levina, X. Wang, S. Hoogland, R. Debnath, L. Brzozowski, E.H. Sargent, J.B. Asbury, Enhanced Mobility-Lifetime Products in PbS Colloidal Quantum Dot Photovoltaics, ACS Nano 6(1) (2012) 89-99.

[20] A.G. Shulga, L. Piveteau, S.Z. Bisri, M.V. Kovalenko, M.A. Loi, Double Gate PbS Quantum Dot Field-Effect Transistors for Tuneable Electrical Characteristics, Advanced Electronic Materials 2(4) (2016) 1500467.

[21] S.Z. Bisri, C. Piliego, M. Yarema, W. Heiss, M.A. Loi, Low Driving Voltage and High Mobility Ambipolar Field-Effect Transistors with PbS Colloidal Nanocrystals, Advanced Materials 25(31) (2013) 4309-4314.

[22] Y. Kim, H. Ko, B. Park, Interfacial dynamic surface traps of lead sulfide (PbS) nanocrystals: test-platform for interfacial charge carrier traps at the organic/inorganic functional interface, Journal of Physics D: Applied Physics 51(14) (2018) 145306.

[23] D.V. Talapin, C.B. Murray, PbSe Nanocrystal Solids for n- and p-Channel Thin Film Field-Effect Transistors, Science 310(5745) (2005) 86.

[24] T.P. Osedach, N. Zhao, T.L. Andrew, P.R. Brown, D.D. Wanger, D.B. Strasfeld, L.-Y. Chang, M.G. Bawendi, V. Bulović, Bias-Stress Effect in 1,2-Ethanedithiol-Treated PbS Quantum Dot Field-Effect Transistors, ACS Nano 6(4) (2012) 3121-3127.

[25] F. Hetsch, N. Zhao, S.V. Kershaw, A.L. Rogach, Quantum dot field effect transistors, Materials Today 16(9) (2013) 312-325.

[26] Y. Liu, J. Tolentino, M. Gibbs, R. Ihly, C.L. Perkins, Y. Liu, N. Crawford, J.C. Hemminger, M. Law, PbSe Quantum Dot Field-Effect Transistors with Air-Stable Electron Mobilities above 7 cm2 V–1 s–1, Nano Letters 13(4) (2013) 1578-1587.

[27] M.I. Nugraha, R. Häusermann, S.Z. Bisri, H. Matsui, M. Sytnyk, W. Heiss, J. Takeya, M.A. Loi, High Mobility and Low Density of Trap States in Dual-Solid-Gated PbS Nanocrystal Field-Effect Transistors, Advanced Materials 27(12) (2015) 2107-2112.

[28] A.G. Shulga, S. Kahmann, D.N. Dirin, A. Graf, J. Zaumseil, M.V. Kovalenko, M.A. Loi, Electroluminescence Generation in PbS Quantum Dot Light-Emitting Field-Effect Transistors with Solid-State Gating, ACS Nano 12(12) (2018) 12805-12813.

[29] D. A. Vithanage , A. Devizis, V. Abramavicius, Y. Infahsaeng, D. Abramavicius, R.C.I. MacKenzie, P.E. Keivanidis, A. Yartsev , D. Hertel, J. Nelson, V. Sundstrom, and V. Gulbinas, Visualizing charge separation in bulk heterojunction organic solar cells, Nature Communication 4 (2011) 2334.

[30] E. Radziemsk, The effect of temperature on the power drop in crystalline silicon solar cells, Renewable Energy 28(1) (2003) 1-12.

[31] W.-k. Koh, S.R. Saudari, A.T. Fafarman, C.R. Kagan, C.B. Murray, Thiocyanate-Capped PbS Nanocubes: Ambipolar Transport Enables Quantum Dot Based Circuits on a Flexible Substrate, Nano Letters 11(11) (2011) 4764-4767.

[32] B. Ding, T. Gao, Y. Wang, D.H. Waldeck, P.W. Leu, J.-K. Lee, Synergistic effect of surface plasmonic particles in PbS/TiO2 heterojunction solar cells, Solar Energy Materials and Solar Cells 128 (2014) 386-393.

[33] Z. Li, F. Gao, N.C. Greenham, C.R. McNeill, Comparison of the Operation of Polymer/Fullerene, Polymer/Polymer, and Polymer/Nanocrystal Solar Cells: A Transient Photocurrent and Photovoltage Study, Advanced Functional Materials 21(8) (2011) 1419-1431.

[34] S. Nakade, T. Kanzaki, Y. Wada, S. Yanagida, Stepped Light-Induced Transient Measurements of Photocurrent and Voltage in Dye-Sensitized Solar Cells: Application for Highly Viscous Electrolyte Systems, Langmuir 21(23) (2005) 10803-10807.

[35] M.A. Hines, G.D. Scholes, Colloidal PbS Nanocrystals with Size-Tunable Near-Infrared Emission: Observation of Post-Synthesis Self-Narrowing of the Particle Size Distribution, Advanced Materials 15(21) (2003) 1844-1849.

[36] G.S. Han, S. Lee, M.L. Duff, F. Qin, M. Jiang, G. Li, J.-K. Lee, Multi-functional transparent electrode for reliable flexible perovskite solar cells, Journal of Power Sources 435 (2019) 226768.

[37] K. Sungjun, L. Jong-Lam, Design of dielectric/metal/dielectric transparent electrodes for flexible electronics, Journal of Photonics for Energy 2(1) (2012) 1-22.

[38] L. Cattin, E. Jouad, N. Stephant, G. Louarn, M. Morsli, M. Hssein, Y. Mouchaal, S. Thouiri, M. Addou, A. Khelil, J.C. Bernède, Dielectric/metal/dielectric alternative transparent electrode: observations on stability/degradation, Journal of Physics D: Applied Physics 50(37) (2017) 375502.

[39] B. Ding, Y. Wang, P.S. Huang, D.H. Waldeck, J.K. Lee, Depleted Bulk Heterojunctions in Thermally Annealed PbS Quantum Dot Solar Cells, J Phys Chem C 118(27) (2014) 14749-14758.

[40] M.J. Yang, B. Ding, J.K. Lee, Surface electrochemical properties of niobium-doped titanium dioxide nanorods and their effect on carrier collection efficiency of dye sensitized solar cells, Journal of Power Sources 245 (2014) 301-307.

[41] S. Lee, H.S. Roh, G.S. Han, J.K. Lee, Controlled oxidation of Ni for stress-free hole transport layer of large-scale perovskite solar cells, Nano Res 12(12) (2019) 3089-3094.

[42] Z. Xu, J. Wu, T. Wu, Q. Bao, X. He, Z. Lan, J. Lin, M. Huang, Y. Huang, L. Fan, Tuning the Fermi Level of TiO2 Electron Transport Layer through Europium Doping for Highly Efficient Perovskite Solar Cells, Energy Technology 5(10) (2017) 1820-1826.

[43] E.M. Miller, D.M. Kroupa, J. Zhang, P. Schulz, A.R. Marshall, A. Kahn, S. Lany, J.M. Luther, M.C. Beard, C.L. Perkins, J. van de Lagemaat, Revisiting the Valence and Conduction Band Size Dependence of PbS Quantum Dot Thin Films, ACS Nano 10(3) (2016) 3302-3311.

[44] B. Kundu, A.J. Pal, Ligand-Mediated Energy-Level Modification in PbS Quantum Dots as Probed by Density of States (DOS) Spectra, The Journal of Physical Chemistry C 122(21) (2018) 11570-11576.